

Published in final edited form as:

*Small.* 2011 June 20; 7(12): 1647–1652. doi:10.1002/sml.201100012.

## Graphite-Coated Magnetic Nanoparticles as Multimodal Imaging Probes and Cooperative Therapeutic Agents for Tumor Cells

**Dr. Joung Kyu Park,**

Department of Chemistry and Chemical Biology Rutgers, The State University of New Jersey Piscataway, NJ 08854, USA; Center for Nano-Biofusion Research Korea Research Institute of Chemical Technology Daejeon 305–600 Korea

**Jongjin Jung,**

Department of Chemistry and Chemical Biology Rutgers, The State University of New Jersey Piscataway, NJ 08854, USA

**Prasad Subramaniam,**

Department of Chemistry and Chemical Biology Rutgers, The State University of New Jersey Piscataway, NJ 08854, USA

**Birju P. Shah,**

Department of Chemistry and Chemical Biology Rutgers, The State University of New Jersey Piscataway, NJ 08854, USA

**Dr. Cheoljin Kim,**

Department of Chemistry and Chemical Biology Rutgers, The State University of New Jersey Piscataway, NJ 08854, USA

**Dr. Jong Kyo Lee,**

Center for Nano-Biofusion Research Korea Research Institute of Chemical Technology Daejeon 305–600 Korea

**Dr. Jee-Hyun Cho,**

Division of Magnetic Resonance Research Korea Basic Science Institute Ochang 363–883, Korea

**Dr. Chulhyun Lee, and**

Division of Magnetic Resonance Research Korea Basic Science Institute Ochang 363–883, Korea

**Prof. Ki-Bum Lee\***

Department of Chemistry and Chemical Biology Rutgers, The State University of New Jersey Piscataway, NJ 08854, USA

An effective therapeutic approach against cancer typically requires the combination of several modalities, such as chemotherapy, radiation, and hyperthermia. In this regard, the development of multifunctional nanomaterial-based systems with combined therapeutic and molecular imaging capabilities has shown great potential but has not been fully explored. In particular, magnetic nanomaterials have been at the fore-front of cancer research as noninvasive imaging probes as well as multifunctional therapeutics.<sup>[1]</sup> For example, magnetic nanoparticles (MNPs) with appropriate surface modifications have been

successfully applied to deliver therapeutic biomolecules, such as anticancer drugs, antibodies, and siRNAs, to target tumor cells or tissues.<sup>[2]</sup> Moreover, the unique physical and chemical properties of these magnetic nanostructures have enabled their wide applications in cancer imaging and therapy, including magnetic resonance imaging (MRI) and hyperthermia.<sup>[3]</sup> Promising advances have been made in synthesizing multifunctional MNPs from various materials, including metals,<sup>[4]</sup> metal oxides,<sup>[5]</sup> metal alloys,<sup>[6]</sup> and metal-graphitic-shell nanomaterials,<sup>[7]</sup> with different properties. However, current studies are mostly focused on the synthesis and characterization of materials with limited demonstration of their biomedical applications, like molecular imaging and therapy. As a result, research efforts towards developing MNP-based multimodal therapeutics to control the tumor microenvironment are highly limited and have not been fully explored. Therefore, in order to address the challenges of MNP-based therapeutics, as well as to narrow the gap between current nanoparticle-based multimodal imaging approaches and their clinical applications, there is a clear need to synthesize effective chemotherapeutic MNPs and to develop multimodal therapies for targeting specific oncogenes, thereby activating/deactivating corresponding key signaling pathways.

In this Communication, we describe the novel synthesis and a systematic in vitro evaluation and application of multifunctional magnetic nanoparticles (MNPs) with an iron cobalt core and a graphitic carbon shell (FeCo/C) for the targeted delivery of small interfering RNA (siRNA) to tumor cells with a concomitant hyperthermia-based therapy, thereby cooperatively inhibiting proliferation of and inducing apoptosis in tumor cells (Figure 1). In parallel, we also demonstrate that our MNPs can be used as highly sensitive magnetic resonance and Raman imaging probes. As a model study, we used glioblastoma multiforme (GBM) cell lines, the most malignant and difficult-to-treat brain tumor cells. We hypothesized that the targeted delivery of our siRNA-MNP constructs against the oncogenic receptor (EGFRvIII) and subsequent hyperthermal treatment would selectively, as well as cooperatively, damage the tumor cells, resulting in the synergistic inhibition of tumor-cell proliferation and the induction of apoptosis via the deactivation of the PI3K/AKT signaling pathway. Hence, these MNP-based therapeutics could potentially be used for the simultaneous imaging and therapy of malignant tumors both in vitro and in vivo.

Recent efforts in cancer therapy have demonstrated the application of hyperthermia, which involves localized heating of cancerous cells or tissues, as an adjuvant to chemotherapy and radiation to improve their efficacy.<sup>[8]</sup> Hyperthermia typically involves increasing the local temperature of the tumor region to 42–46 °C over a given time period, ultimately resulting in apoptosis of the heat-sensitized cancer cells.<sup>[9]</sup> One of the best methods of achieving a localized hyperthermal effect is to deliver MNPs to the target cells and subsequently apply electromagnetic fields following their cellular uptake/localization.<sup>[10]</sup> Furthermore, hyperthermia and its downstream effects can be significantly enhanced by the concomitant use of other cancer therapies, including radiation and drug/gene delivery and vice versa.

To develop cooperative (hyperthermia and siRNA delivery) therapeutic systems based upon MNPs, we synthesized graphitic-carbon-protected iron cobalt (FeCo/C) nanoparticles (7 and 11 nm in diameter) with a body-centered cubic (bcc) crystalline structure using hydrothermal synthetic methods followed by an annealing process at 1000 °C. High-resolution transmission electron microscopy (HR-TEM) and X-ray diffraction (XRD) confirmed the excellent chemical/physical properties of our FeCo/C NPs, such as monodispersity, narrow size distribution of the nanoparticles, and the presence of a crystalline bcc FeCo core (Figure 2). The graphitic-carbon shells surrounding the FeCo core were confirmed by Raman spectroscopy analysis and HR-TEM. Furthermore, the thickness of the graphitic-carbon coating could be monitored by the intensity of the Raman signal (marked by arrows in Figure 2d). We also characterized the magnetic properties of our

FeCo/C NPs using a superconducting quantum interference device (SQUID). Our FeCo/C NPs were found to display remarkable superparamagnetic properties at room temperature, as suggested by the significantly higher value of the saturation magnetization ( $M_s$  for our FeCo/C NPs as compared to that of the commercially available  $\text{Fe}_3\text{O}_4$  (Figure 2e). This was attributed to the higher magnetic moments of the FeCo/C NPs as a result of the high-temperature annealing, as shown in Figure S2 in the Supporting Information (SI).

In this work, our FeCo/C MNPs have several advantages over other conventional magnetic nanoparticles, such as FePt,  $\text{Fe}_2\text{O}_3$ , and  $\text{Fe}_3\text{O}_4$ : i) FeCo exhibits an excellent magnetization value (e.g., 11-nm FeCo  $\approx 235 \text{ emu g}^{-1}$ ), has a high Curie temperature, and has high magnetic anisotropy energies, all of which are critical in order to enhance their potential for biomedical applications, such as MRI and hyperthermia; ii) the thickness of the outer graphite-shell layers can be controlled by our synthetic method, which would lead to an improved Raman signal intensity for detecting cancerous cells; and iii) the nanoparticles are chemically inert due to the presence of a graphitic carbon shell [11] and can be made biocompatible by appropriate surface modifications (e.g., dextran-ligand coating). Moreover, compared to conventional methods [1b,12] for the synthesis of core-shell metal-alloy magnetic nanomaterials, such as electric-arc discharge, [13] high-temperature thermal decomposition, [14] and chemical vapor deposition (CVD), [11] our novel hydrothermal synthetic approach has several advantages, such as relatively milder synthetic conditions, low environmental impact, cost effectiveness, ease of scalability (see Figure S3 in the SI), and the exclusion of toxic solvents and size-separation techniques.

Another critical step to realize the full potential of our multimodal FeCo/C NPs for in vitro/ in vivo biomedical applications (e.g., targeted drug/gene delivery, MRI, or hyperthermal therapy) is to make the nanoparticles biocompatible and modify the surface for achieving target-specific intracellular delivery. [15] Several strategies, including coating with molecules such as dextran, have been successfully used for functionalizing magnetic nanoparticles and rendering them biocompatible. [16] Hence, we synthesized a series of dextran derivatives (see Figure S4a in the SI) and used them to coat our FeCo/C NPs (see Figure S4b in the SI). The dextran-coated FeCo/C NPs were found to have excellent colloidal stability and the hydro-dynamic diameter was found to be  $\approx 150 \text{ nm}$  (see Figures S5 and S6 in the SI). These dextran-modified FeCo/C NPs were then conjugated to specific cancer-targeting biomolecules, such as epidermal growth factor receptor (EGFR) antibodies and cyclic-RGD (c-RGD) peptide, to target glioblastoma cells and to improve their intracellular uptake. The conjugation of biomolecules such as EGFR antibodies and c-RGD to our FeCo/C NPs not only increases transfection of our nanoparticles via receptor-mediated endocytosis but can also selectively target the glioblastoma cells by binding to receptors (EGFR and integrins) known to be overexpressed in glioblastoma cells. [17]

Highly sensitive multimodal imaging tools like MRI, computed tomography (CT), positron-emission tomography (PET), and Raman imaging, which rely on nanomaterials as molecular probes, have gained much attention as diagnostic tools for specific cancers, such as breast and brain cancers. [18] In order to investigate the capability of our FeCo/C NPs as multimodal imaging nanoprobe, we focused on two important imaging methods for cancer, in vivo MRI and in vitro Raman imaging, both of which provide complementary information about tumor microenvironments at the tissue level and/or cellular level. [3b,18b] In order to test the capability of our MNPs as MRI contrast agents, the transverse relaxation times ( $T_2$ ) of the water protons were measured in a specific magnetic field and their values were compared to those of the commercially available MRI contrast agent Resovist ( $\text{Fe}_3\text{O}_4$ , from Roche). Both the 7- and 11-nm FeCo/C NPs exhibited a higher relaxivity coefficient ( $r_2$ , 252 and  $392 \text{ m M}^{-1} \text{ s}^{-1}$ , respectively) and enhanced  $T_2$ -weighted MR contrast (Figure 3a,b) as compared to Resovist ( $r_2 = 140 \text{ m M}^{-1} \text{ s}^{-1}$ ). Characterization of our biocompatible

dextran-coated FeCo/C NPs as in vivo MRI agents was performed by injecting the MNPs into a rat's tail vein. Preliminary MRI studies showed that our nanoparticles accumulated in the liver, spleen, and kidneys and their imaging contrast was significantly higher (about 10 times) than that of Resovist (Figure 3c). We also monitored the in vivo biodistribution and MRI contrast of these FeCo/C NPs over 10 days. It was found that the NPs were retained in the liver and spleen and that there was no significant loss of imaging contrast over this time period (see Figure S7 in the SI). Furthermore, the analysis of in vitro Raman imaging results, wherein confocal microscopy was used to observe the NP-internalized U87 cell lines, confirmed that the intensity of the D and G bands of the graphitic-carbon shells was indeed proportional to the thickness of the carbon shells on the FeCo/C NPs (Figure 3d). This data strongly suggests that our FeCo/C NPs have a well defined correlation and sensitive response when used as Raman imaging probes at the single-cancer-cell level. These preliminary in vitro and in vivo studies showed no visible cytotoxicity due to the degradation of the FeCo/C NPs. It has been reported that FeCo/C NPs are safely excreted over time through the biliary system after being taken up by the liver and spleen.<sup>[19]</sup> Hence, it is highly unlikely that these FeCo/C NPs would pose any serious toxicity issues when used in vivo. A detailed toxicological evaluation of these MNPs in animal models would be forthcoming in the future.

Having demonstrated the potential of our FeCo/C NPs as multimodal imaging probes, we then focused on evaluating their ability to be used as targeted hyperthermia agents for tumor therapy in vitro. We hypothesized that our FeCo/C NPs would be more efficient hyperthermia agents than Fe<sub>3</sub>O<sub>4</sub> NPs of similar size due to their high magnetization and therefore would be more effective in inhibiting proliferation and inducing apoptosis of target brain tumor cells (bTCs). To test their efficacy as targeted hyperthermia agents, we first measured the minimum time required to attain the therapeutic temperature ( $\approx 43^\circ\text{C}$ ) when placed in a homogeneous magnetic field. The specific absorption rates (SARs) of FeCo/C and Fe<sub>3</sub>O<sub>4</sub> NPs ( $\approx 69\text{ W g}^{-1}$  for FeCo/C and  $13\text{ W g}^{-1}$  for Fe<sub>3</sub>O<sub>4</sub>), as derived from the plots of temperature versus time in aqueous solutions under a 334 kHz magnetic field (which is the optimum frequency range estimated by the Neel and Brownian relaxation-time simulations<sup>[20]</sup>), indicated that the time required for our FeCo/C NPs to reach the therapeutic temperature was ten times shorter than that of Fe<sub>3</sub>O<sub>4</sub> NPs (see Figure S9 in the SI). We next evaluated the concentration-dependent cytotoxicity of our FeCo/C NPs by serial-dilution investigations. From this study, the range of concentrations inducing negligible cytotoxic effects on cells was identified and the concentrations (95% cell viability at  $300\text{ }\mu\text{g mL}^{-1}$  after  $\approx 24\text{ h}$  post transfection) within this range were used for our subsequent experiments (see Figure S10 in the SI). We then sought to precisely increase the temperature of tumor cells while minimizing the exposure of other cells to hyperthermic temperatures. For this purpose, FeCo/C NPs functionalized with c-RGD peptide or EGFR antibodies were incubated in cocultures of glioblastoma cells (U87–EGFP), which had been genetically labeled with enhanced green fluorescent protein (EGFP) and present EGFRs on their membranes and several other less tumorigenic cells, such as PC-12 and astrocytes, which tend to have low expression levels of integrins and EGFRs. Our data clearly indicates that the surface modification of our FeCo/C NPs with c-RGD peptide or EGFR antibodies resulted in their selective cellular uptake by the target bTCs, as compared to PC-12 or astrocytes (see Figure S11 in the SI). Following intracellular uptake of the aforementioned NP constructs, the cells were exposed to an alternating current (AC) magnetic field for 15 min. Significant inhibition of proliferation and hyperthermia-induced cell death was observed mainly in the U87 cells while the less-tumorigenic PC-12 cells largely continued proliferating with time (**Figure 4a,b**).

In the past decade, there has been considerable interest in the development of nanoparticle-based siRNA-delivery methods for cancer therapy. RNA interference (RNAi) involves the

use of siRNAs to selectively mediate the cleavage of complementary mRNA sequences and thus regulate target gene expression.<sup>[21]</sup> In combination with other chemotherapeutic methods like hyperthermia, RNAi could prove to be a powerful tool to manipulate the tumor microenvironment. In order to deliver siRNA to the target cells, the FeCo/C NPs were conjugated to the siRNA using polyethyleneimine (PEI) as a cationic polymer via a layer-by-layer approach<sup>[22]</sup> (see Figure S13 in the SI). We initially optimized the knockdown efficiency of our siRNA–FeCo/C NP construct by the suppression of EGFP in U87–EGFP cells. The decrease in green fluorescence intensity due to siRNA-mediated knockdown of EGFP was monitored to assess the knockdown efficiency ( $\approx 80\%$  after 3 days of transfection) of our siRNA–NP constructs (see Figure S14 in the SI). Once the conditions for the siRNA delivery and knockdown were optimized, we focused on inhibiting the proliferation and inducing apoptosis of U87–EGFRvIII cell lines overexpressing the oncogenic EGFRvIII gene. EGFRvIII is a mutant type of EGFR as well as an oncogenic receptor that is highly expressed only in tumor cells, and not in normal cells.<sup>[23]</sup> The effect of the knockdown of the EGFRvIII oncogene using our siRNA–FeCo/C NP constructs was assessed using a microscope at 96 h post transfection (see Figure S14 in the SI). We hypothesized that the knockdown of the target oncogene, EGFRvIII, with our multifunctional siRNA–FeCo/C NP constructs, combined with hyperthermia, would lead to a cooperative inhibition of tumor-cell proliferation and increase in cell death. The U87–EGFRvIII cells were incubated with our FeCo/C NPs modified with siRNA against EGFRvIII, followed by hyperthermia treatment for 5 min at 72, 96, and 120 h post siRNA treatment. Quantitative analysis based upon the 3-(4,5-dimethylthiazol-2-yl)-5-(3-carboxymethoxyphenyl)-2-(4-sulfophenyl)-2H-tetrazolium assay, commonly known as the MTS assay (Figure 4c) showed that treatment of cells with our siRNA–MNPs against EGFRvIII followed by hyperthermia induced significantly more cell death as compared to the controls. This could be attributed to the fact that silencing of the EGFRvIII oncogene results in a decrease in expression of the focal adhesion proteins that make the cells more susceptible to heat, thereby leading to a synergistic increase in cell death.<sup>[24]</sup> Our study clearly demonstrates that the appropriate combination of various therapeutic modalities using our FeCo/C NPs can significantly enhance the therapeutic efficacy relative to the individual components.

In summary, this work provides an early demonstration of integrating multimodal imaging with combined hyperthermia and siRNA-based therapy in malignant tumor cells using highly efficient FeCo/C NPs. Our FeCo/C NPs have successfully been demonstrated to have a well defined correlation and a fast and sensitive thermal response to the strength of the applied magnetic field. At the same time, our FeCo/C NPs could be developed as novel therapeutic and diagnostic tools for cancer research. The ability to functionalize the graphitic surface of the FeCo/C NPs with targeting ligands and biomolecules would be critical to realize the potential of nanoparticle-based diagnosis and therapy of various cancers. It should be noted that our FeCo/C NPs showed excellent MRI contrast results compared to the conventional MRI contrast agents as well as enabling us to collect the Raman spectral information at the single-cell level. More importantly, the use of our FeCo/C NPs for site-specific and localized hyperthermia in conjunction with siRNA therapy against oncogenes would greatly complement and enhance the effects of other therapeutic modalities, including gene therapy and chemotherapy, thereby reducing the dose of anticancer drugs, mitigating their toxic side effects, and effectively circumventing drug resistance in cancers.

## Supplementary Material

Refer to Web version on PubMed Central for supplementary material.

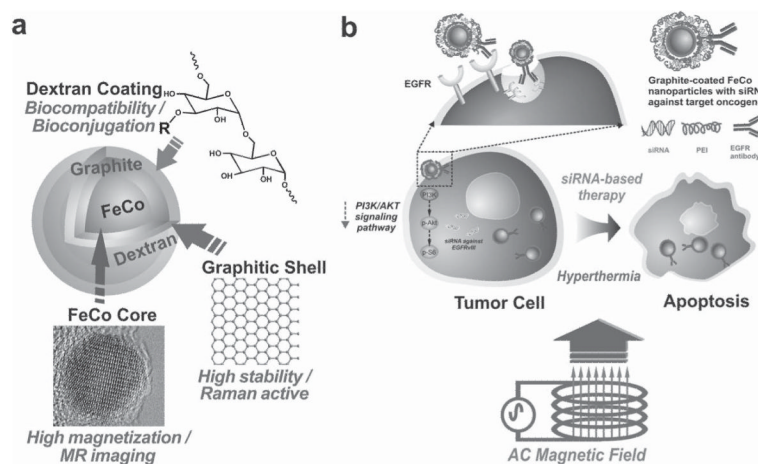
## Acknowledgments

We thank Prof. Huixin He for helping us with the hyperthermia studies, Prof. Sang-Wook Cheong and Prof. Martha Greenblatt for their support for the SQUID measurements and the IAMDN center for allowing us to use their high-resolution TEM facility. We are grateful to the KBLEE group members (Aniruddh Solanki, Shreyas P. Shah, and Michael Koucky) for their valuable suggestions for the manuscript. J.K.P. acknowledges the research program at KRICT and Dr. Young-Duk Suh and Dr. Kee-Suk Jun for the Raman imaging. K.-B.L. acknowledges the NIH Director's Innovator Award (1DP20D006462-01) and is also grateful to the N.J. Commission on Spinal Cord Research grant (09-3085-SCR-E-0).

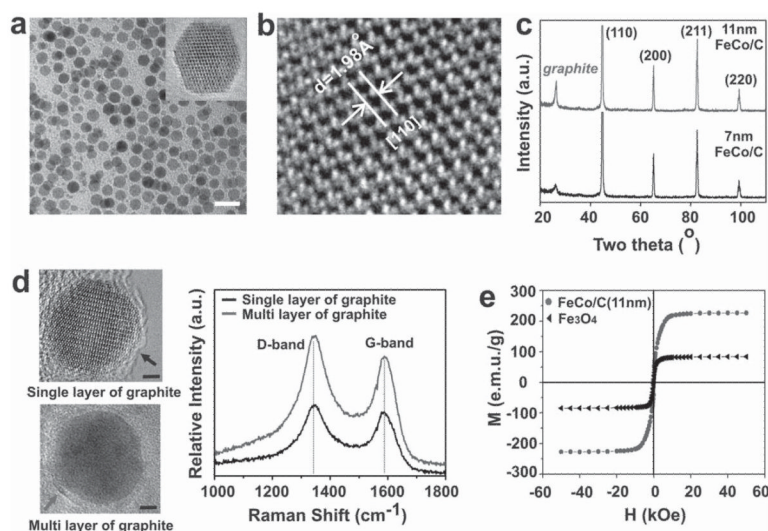
## References

- [1] a). Bulte JWM, Douglas T, Witwer B, Zhang SC, Strable E, Lewis BK, Zywicke H, Miller B, van Gelderen P, Moskowitz BM, Duncan ID, Frank JA. *Nat. Biotechnol.* 2001; 19:1141–1147. [PubMed: 11731783] b) Lu AH, Salabas EL, Schuth F. *Angew. Chem. Int. Ed.* 2007; 46:1222–1244.c) Zeng H, Sun SH. *Adv. Funct. Mater.* 2008; 18:391–400.d) Solanki A, Kim JD, Lee KB. *Nanomedicine.* 2008; 3:567–578. [PubMed: 18694318]
- [2] a). Gao JH, Gu HW, Xu B. *Acc. Chem. Res.* 2009; 42:1097–1107. [PubMed: 19476332] b) Hu SH, Kuo KT, Tung WL, Liu DM, Chen SY. *Adv. Funct. Mater.* 2009; 19:3396–3403.
- [3] a). Kim J, Lee JE, Lee SH, Yu JH, Lee JH, Park TG, Hyeon T. *Adv. Mater.* 2008; 20:478–483.b) Lin WB, Hyeon T, Lanza GM, Zhang MQ, Meade TJ. *MRS Bulletin.* 2009; 34:441–448.c) Hogemann D, Ntziachristos V, Josephson L, Weissleder R. *Bioconj. Chem.* 2002; 13:116–121.
- [4]. Huber DL. *Small.* 2005; 1:482–501. [PubMed: 17193474]
- [5]. Lee H, Yu MK, Park S, Moon S, Min JJ, Jeong YY, Kang HW, Jon S. *J. Am. Chem. Soc.* 2007; 129:12739–12745. [PubMed: 17892287]
- [6]. Sun SH, Murray CB, Weller D, Folks L, Moser A. *Science.* 2000; 287:1989–1992. [PubMed: 10720318]
- [7]. Mahmood M, Xu Y, Li ZR, Dervishi E, Ali N, Saini V, Biris AS, Trigwell S, Zharov VP, Biris AR. *IEEE Trans. Ind. Appl.* 2009; 45:2162–2169.
- [8]. Huilgol NG, Gupta D, Dixit R. *Int. J. Hyperther.* 2010; 26:21–25.
- [9]. Prasad NK, Rathinasamy K, Panda D, Bahadur D. *J. Mater. Chem.* 2007; 17:5042–5051.
- [10] a). Cherukuri P, Glazer ES, Curley SA. *Adv. Drug Deliv. Rev.* 2010; 62:339–345. [PubMed: 19909777] b) Ito A, Matsuoka F, Honda H, Kobayashi T. *Canc. Gene Ther.* 2003; 10:918–925.
- [11] a). Seo WS, Kim SM, Kim YM, Sun X, Dai HJ. *Small.* 2008; 4:1968–1971. [PubMed: 18752210] b) Seo WS, Lee JH, Sun XM, Suzuki Y, Mann D, Liu Z, Terashima M, Yang PC, McConnell MV, Nishimura DG, Dai HJ. *Nat. Mater.* 2006; 5:971–976. [PubMed: 17115025]
- [12] a). Park J, An KJ, Hwang YS, Park JG, Noh HJ, Kim JY, Park JH, Hwang NM, Hyeon T. *Nat. Mater.* 2004; 3:891–895. [PubMed: 15568032] b) Bystrzejewski M, Huczko A, Lange H, Baranowski P, Cota-Sanchez G, Soucy G, Szczytko J, Twardowski A. *Nanotechnology.* 2007; 18:145608.c) Hyeon T, Lee SS, Park J, Chung Y, Bin Na H. *J. Am. Chem. Soc.* 2001; 123:12798–12801. [PubMed: 11749537]
- [13]. Dong XL, Zhang ZD, Jin SR, Kim BK. *J. Appl. Phys.* 1999; 86:6701–6706.
- [14] a). Yamada M, Okumura SJ, Takahashi K. *J. Phys. Chem. Lett.* 2010; 1:2042–2045.b) Behrens S, Bonnemann H, Matoussevitch N, Gorschinski A, Dinjus E, Habicht W, Bolle J, Zinoveva S, Palina N, Hormes J, Modrow H, Bahr S, Kemper V. *J. Phys. Condens. Matter.* 2006; 18:S2543–S2561.
- [15]. Zhang Y, Kohler N, Zhang MQ. *Biomaterials.* 2002; 23:1553–1561. [PubMed: 11922461]
- [16] a). Berry CC, Wells S, Charles S, Aitchison G, Curtis ASG. *Biomaterials.* 2004; 25:5405–5413. [PubMed: 15130725] b) Hifumi H, Yamaoka S, Tanimoto A, Akatsu T, Shindo Y, Honda A, Citterio D, Oka K, Kuribayashi S, Suzuki K. *J. Mater. Chem.* 2009; 19:6393–6399.
- [17]. Xie J, Chen K, Lee HY, Xu CJ, Hsu AR, Peng S, Chen XY, Sun SH. *J. Am. Chem. Soc.* 2008; 130:7542–7543. [PubMed: 18500805]
- [18] a). Lee H, Lee E, Kim DK, Jang NK, Jeong YY, Jon S. *J. Am. Chem. Soc.* 2006; 128:7383–7389. [PubMed: 16734494] b) Qian XM, Peng XH, Ansari DO, Yin-Goen Q, Chen GZ, Shin DM, Yang L, Young AN, Wang MD, Nie SM. *Nat. Biotechnol.* 2008; 26:83–90. [PubMed: 18157119]

- c) Haka AS, Shafer-Peltier KE, Fitzmaurice M, Crowe J, Dasari RR, Feld MS. *Cancer Res.* 2002; 62:5375–5380. [PubMed: 12235010]
- [19]. Lee JH, Sherlock SP, Terashima M, Kosuge H, Suzuki Y, Goodwin A, Robinson J, Seo WS, Liu Z, Luong R, McConnell MV, Nishimura DG, Dai H. *Magn. Reson. Med.* 2009; 62:1497–1509. [PubMed: 19859938]
- [20]. Mornet S, Vasseur S, Grasset F, Duguet E. *J. Mater. Chem.* 2004; 14:2161–2175.
- [21]. Jung JJ, Solanki A, Memoli KA, Kamei K, Kim H, Drahl MA, Williams LJ, Tseng HR, Lee K. *Angew. Chem. Int. Ed.* 2010; 49:103–107.
- [22]. Elbakry A, Zaky A, Liebk R, Rachel R, Goepferich A, Breunig M. *Nano Lett.* 2009; 9:2059–2064. [PubMed: 19331425]
- [23]. Gan HK, Kaye AH, Luwor RB. *J. Clinical Neurosci.* 2009; 16:748–754. [PubMed: 19324552]
- [24]. Ning Y, Zeineldin R, Liu YY, Rosenberg M, Stack MS, Hudson LG. *Canc. Res.* 2005; 65:9280–9286.

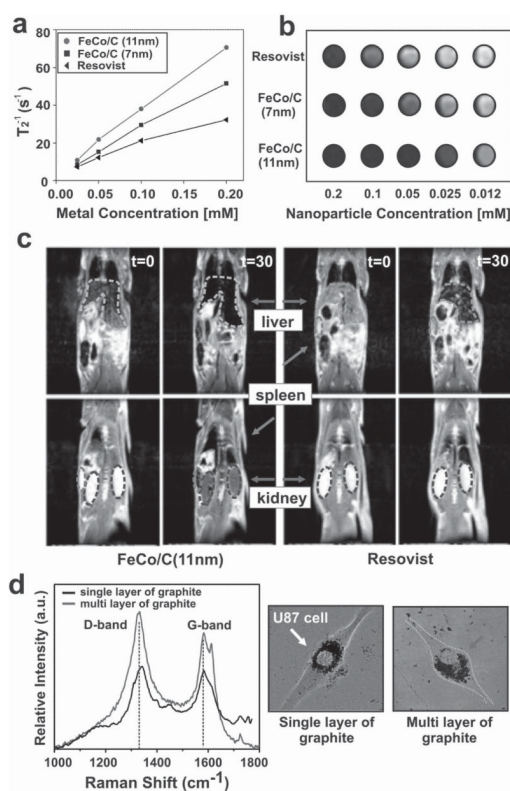


**Figure 1.** Magnetic FeCo-graphite nanoparticles for multimodal imaging and targeted tumor therapy. a) Detailed structure of the MNPs depicting the highly magnetic FeCo core, protective Raman-active graphite shell, and the biocompatible dextran coating. b) Inhibition of proliferation and induction of apoptosis via combined siRNA delivery and hyperthermia using siRNA-FeCo/C NP constructs.



**Figure 2.**

Structural and magnetic properties of the FeCo/C nanoparticles. a) TEM image of the 11-nm nanoparticles (scale bar = 20 nm). b) HR-TEM image of the nanoparticles showing the crystalline lattice structure of the FeCo core. c) Powder XRD for the 7- and 11-nm nanoparticles showing the presence of a bcc crystalline core and graphitic shell. d) Raman spectrum (excitation at 632.8 nm) of the 11-nm nanoparticles with single and multiple carbon shells (marked by arrows) showing the D and G bands of graphitic carbon (scale bar = 2 nm). e) Room-temperature magnetization versus applied magnetic field for 11-nm FeCo/C NPs (red symbols) and  $\text{Fe}_3\text{O}_4$  (black symbols). Note that no hysteresis loop exists owing to the superparamagnetism of the nanoparticles.

**Figure 3.**

MR measurements and imaging of FeCo/C NPs and Resovist. a) Concentration-dependent  $T_2$  measurements of FeCo/C NPs and Resovist solutions. b)  $T_2$ -weighted MR images of various nanoparticle solutions. The FeCo/C NPs show higher MR image contrast (several fold) as compared to Resovist, a traditional MRI contrast agent. c)  $T_2$ -weighted MR images of a rat before ( $t = 0$  min) and 30 min after ( $t = 30$  min) injection of FeCo/C NPs (left) and Resovist (right) into a rat's tail vein. The nanoparticles were seen to localize in the liver (green arrow), spleen (blue arrow), and kidneys (red arrow) of the animal. Also, FeCo/C NPs show a higher imaging contrast at a lower concentration (0.25 mg of Fe) as compared to Resovist (2.5 mg of Fe). d) Raman spectra of U87-EGFP cells (marked by arrows) treated with 11-nm FeCo/C NPs. The spectra shows the capability of the FeCo/C NPs to be used as imaging agents at the single-cell level (see Figure S8 in the SI for detailed Raman imaging).

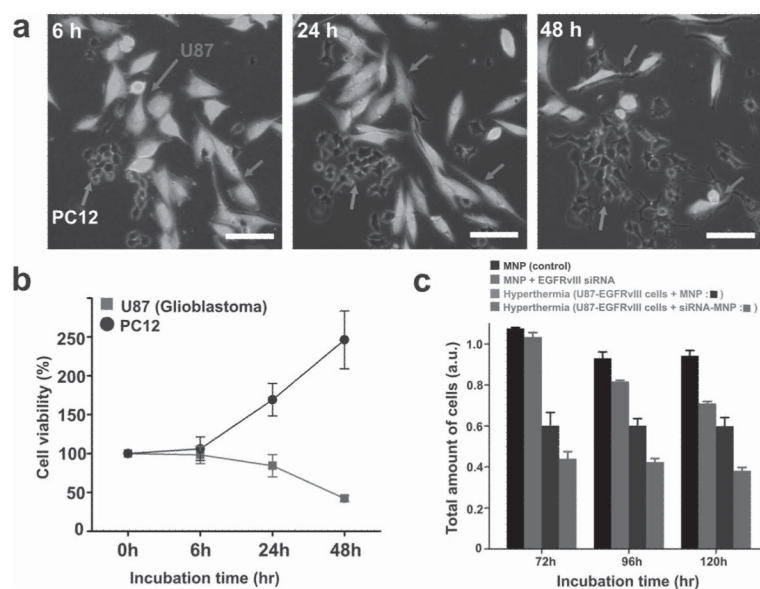


**Figure 4.**

In vitro hyperthermia and siRNA-delivery studies of the FeCo/C NPs. a,b) U87-EGFP cell death induced by hyperthermia in cocultures of the highly tumorigenic U87-EGFP cells (marked by arrows) and the less-tumorigenic PC-12 cells (marked by arrows) via the targeted delivery of FeCo/C NPs to the U87 cells. Fluorescence images (a) and quantitative analysis (b) show that significant hyperthermia-induced cell death is observed in U87 cells, while the PC-12 cells keep proliferating with time. (Note that the number of cells at 0 h was taken to be 100% and the cell counts at other time points were normalized to this value.) Annexin V assays for detection of early apoptosis proved that the cell death was caused by localized hyperthermia-induced apoptosis rather than necrosis (see Figure S12 in the SI). c) MTS assay demonstrating the synergistic inhibition of proliferation and induction of cell death by the combined siRNA and hyperthermia treatment using siRNA-FeCo/C NPs in U87-EGFRvIII cells as compared to individual treatments and nontreated controls. The scale bar in all images is 100  $\mu$ m.